Electrochemically Activated Histidine-tagged Flavoenzyme-mediated Biopseudocapacitor

Suhwan Sung
Kyonggi University
Joon-Hyung Jin
jjh1023@kgu.ac.kr

Kyonggi University https://orcid.org/0000-0002-8525-0740

Research Article

Keywords: biopseudocapacitor, electric double-layer capacitor, enzyme-linked supercapacitor, ferricyanide-labeled enzyme, histidine-tagged enzyme

Posted Date: December 20th, 2023

DOI: https://doi.org/10.21203/rs.3.rs-3723159/v1

Version of Record: A version of this preprint was published at Korean Journal of Chemical Engineering on April 1st, 2024. See the published version at https://doi.org/10.1007/s11814-024-00164-8.

Abstract

Polypeptides or enzyme proteins have specific functions depending on their unique three-dimensional structures. Active-site histidine or histidine tags in an enzyme protein can be used to fix an electrochemically active species to the enzyme and can be further used as an electroactive material for the electrode substrate of a faradaic supercapacitor, which is an energy storage device with high power density. Here, we introduce an enzyme-linked electric double-layer capacitor and a pseudocapacitor prepared by cyclovoltametrically intercalating histidine moieties of the linked enzymes with ferricyanide ions. Indium tin oxide (ITO) was employed as the electrode substrate for immobilization of histidine-tagged methyl tryptophan oxidase (HMTO). After attaching HMTO via amino-glutaraldehyde cross-linking chemistry, the resulting HMTO-ITO electrodes were further activated with ferricyanide. The approximate amount of HMTO immobilized on an ITO substrate of area 1.13 cm^2 was 3.3 ± 0.46 μC, equivalent to 11.4 pmole (0.49 μg) of HMTO. The specific capacity of the biopseudocapacitor determined using cyclic voltammetry was 6.19 C g^{-1} at a scan rate of 10 mV s^{-1}.

1. Introduction

Supercapacitors have been widely employed in various industrial applications that require a high electric power for a relatively short period of time, a high number of charge/discharge cycles, and a long lifetime, such as handheld tools, renewable or sustainable energy harvest/storage, ground-based transportation vehicles, and even aerial vehicles. These supercapacitors or electrochemical capacitors, belonging to a group of energy storage devices with a power density higher than that of the conventional secondary battery, are divided into three major categories: electric double-layer capacitor (EDLC), pseudocapacitors, and hybrid capacitors [1–6]. While the EDLC stores most of the electrical energy through electrostatic double-layer capacitance and shows excellent charging/discharging cyclability with theoretical unlimited lifetime, pseudocapacitors store energy by means of faradaic pseudocapacitance in addition to static double-layer capacitance, and therefore show greater energy storage capability than the EDLC [7]. More importantly, in many cases, pseudocapacitors composed of organic polymeric conductors [2] and metal oxide nanopowders [1, 3] are intrinsically compatible with recently developed stretchable and wearable electronics. However, the working mechanisms involving redox reactions, which are detrimental to the device lifetime, restrict the employment of pseudocapacitors to some state-of-the-art research fields only. Although we have previously reported mechanically fixed electroactive metal oxide nanopowders in a stretchable pseudocapacitor yarn [8], effective and strong fixation of electroactive materials to the electrode substrate of energy storage devices is still challenging.

In recent years, enzyme-based biosupercapacitors have been introduced [9–16]. In this work, a biopseudocapacitor shows hybrid charge storage properties, i.e., electric double-layer capacity and pseudocapacity, simultaneously. We report a bioelectrode with pseudocapacitive properties based on a histidine-tagged N-methyl tryptophan oxidase (HMTO)-mediated ferricyanide/ferrocyanide as the electroactive redox species. A flavoenzyme group, including the N-methyltryptophan oxidase and sarcosine oxidase, commonly contains active-site histidines [17, 18], and the histidine residue, a versatile

amino acid in an enzyme, can strongly bind to electroactive metal complexes [19–22]. Herein, we describe the development of an electroactive ferricyanide-linked HMTO-mediated pseudocapacitive electrode utilizing glutaraldehyde cross-linking of the HMTO enzyme onto indium tin oxide (ITO) electrodes treated with (3-aminopropyl)triethoxysilane (APTES). The materials and methods used in this work are technically compatible with stretchable and wearable electronics. Our approach also proves the effectiveness and usefulness of the employment of an enzyme to fix electroactive materials to an energy storage electrode.

The HMTO-entrapped biopseudocapacitor electrode was characterized using electrochemical impedance spectroscopy (EIS), cyclic voltammetry (CV), attenuated total reflectance Fourier-transform infrared spectroscopy (ATR-FTIR), Raman spectroscopy, and atomic force microscopy (AFM) throughout the biopseudocapacitor assembly.

3. Results and discussion

3.1. Spectroscopic and surface analyses

The bare ITO surface becomes rougher as the surface is consecutively modified with various chemicals including HMTO molecules on the surface. According to AFM data, as shown in Fig. 2, the root-mean-square roughness of the bare ITO surface, which is approximately 4.03 nm, increases to 7.56 nm after the HMTO is immobilized. The corresponding ATR-FTIR spectra confirm that the ITO substrate is correctly modified. Hydroxyl groups on the HO-ITO electrode, which are available for hydrogen bonding between adjacent hydroxyl groups, show a broad peak at approximately 3428 cm^{-1} [23, 24]. A broad stretching vibration peak of the primary amine group of APTES-ITO is observed at 3440 cm^{-1} [16, 25–27]. An imine vibration band v(C = N) owing to cross-linked amino-GA and GA-HMTO junctions shows a sharp peak at 1639 cm^{-1} via ATR-FTIR, which is also observed at 1610 cm^{-1} in the Raman spectra with a more enhanced Raman intensity in the case of HMTO-ITO, as shown in Fig. S2 (Supporting Information) [28]. Stretching vibration peaks related to the amide bonds within the immobilized HMTO molecules are shown at 1540 (N-H bending, overlapped), 1650 (C = O stretching, overlapped), and 3300 cm^{-1} (N-H stretching) [29–31]. Si-O stretching and O-Si-O asymmetric stretching vibrations of siloxane bonds are observed at 1046 and 1109 cm^{-1}, respectively. The two peaks shown at 2852 and 2927 cm^{-1} are assigned to the C-H stretching vibrations of the alkyl and alkoxy hydrocarbons [32]. Note that the v(C = N) bands shown in both the ATR-FTIR and the Raman spectra of GA-ITO are enhanced after HMTO immobilization. This indicates that a primary amine group on the HMTO molecule has formed an imine linkage with the immobilized amino-glutaraldehyde group.

3.2. Electrochemical impedance spectroscopic characterization

Figure 3 shows the EIS spectra of bare ITO, HO-ITO, APTES-ITO, GA-ITO, and HMTO-ITO substrates in the presence of the redox couple. The first three electrodes show traditional Randles behavior [33], i.e., a solution resistance (R_s) in series with a parallel circuit of double-layer capacitor (C_d) and a charge-transfer resistance (R_{ct}) in series with Warburg impedance (W). While R_s varies randomly with the resistance of the electrolyte, the contact resistances of the Teflon® cell, and the intrinsic resistance of the modified ITO film [34], R_{ct} decreases from 579 Ω for bare ITO to 33 Ω for APTES-ITO with the progress in the modification procedure. This indicates that the charge transfer reaction of the redox couple on the APTES-ITO surface is kinetically more facile than that on the bare ITO surface. More interestingly, the EIS spectra of GA-ITO and HMTO-ITO have a linear region of Z" as a function of Z' in the high-frequency regime, possibly owing to their polymer-like surface structure expressed by the Warburg impedance in the polymer network [35–37]. Notably, the HMTO purification tag, which contains six histidine residues on the terminal end of HMTO, can form multiple coordination bonds with ferricyanides [38, 39].

The same R_s of various electrodes was observed in the EIS spectra obtained in the absence of the redox couple (V_{DC} = -0.6 V vs. Ag/AgCl) as shown in Fig. 4. The equivalent circuit for the EIS spectra is composed of three elements: R_s, C_d, and an inductance (L) [34]. Note that the Warburg impedance is not shown in Fig. 4 because the electrolyte solution does not contain any electrochemical active species. The observation of inductive elements in the EIS spectra—as attributed to the relaxation process of the surface adsorbates depending on the applied bias, assuming that the adsorbates follow the Langmuir adsorption isotherm—has been proven previously through experiments and computer simulations [40–42]. The corresponding phase diagrams shown in Fig. S3 (Supporting Information) present the capacitive behavior of bare ITO, which is confirmed by the phase angle of 82° observed in the low-frequency region. Both hydroxylation and silanization of ITO resulted in a peak of phase angle at approximately 10 Hz, and the peak frequency was downshifted by modification processes such as amino-aldehyde cross-linking and HMTO immobilization; however, the phase shift was strongly dependent on the applied bias [43]. All the electrodes acted as capacitors when V_{DC} was 0 V, and no peak frequency was observed (Fig. S4, Supporting Information).

3.3. Voltammetric characterization

Figure 5 presents the CV diagrams of various electrode substrates in the presence of the redox couple. The anodic faradaic peak (i_a) and cathodic peak (i_c) currents of the bare ITO increased significantly after the electrode surface was hydroxylated and subsequently silanized with APTES, thereby indicating that the hydrophilic HO-ITO and APTES-ITO surfaces were electrochemically more favorable for the redox reaction of electroactive species. In contrast, the GA-ITO surface was more efficiently passivated and shows that the faradaic reaction was suppressed and the corresponding current flow considerably decreased simultaneously. According to the semi-empirical Randles–Sevcik equation, $i_p = (2.69\times10^5)n^{3/2}\cdot A\cdot D^{1/2}\cdot C^*\cdot v^{1/2}$ (where i_p, n, A, D, C^*, and v represent the peak current, number of electrons involved in the reaction, active area of the electrode, diffusion coefficient (assumed as 7.6×10^{-6} cm^2 s^{-1}

for both ferricyanide and ferrocyanide ions) [44], bulk concentration of the electroactive species, and potential scan rate, respectively), the calculated electrochemical active areas of each electrode based on the anodic Randles' plots were 0.36 cm^2 for bare ITO, 0.65 cm^2 for HO-ITO, 0.90 cm^2 for APTES-ITO, and 0.05 cm^2 for GA-ITO. This indicates that only 4.3% of the area of the GA-ITO electrode is electrochemically active as compared with the geometric area of the bare ITO electrode, which suggests that the ITO surface is sufficiently covered with GA.

Figure 6a displays the CV diagrams for various electrode substrates, including that of the HMTO-ITO electrode in the PBS solution excluding the redox couple. We observe that each of the electrodes exhibits predominantly capacitive current flows with negligible amounts of faradaic current as in an ideal EDLC capacitor. The active site of HMTO does contain an electrochemically active prosthetic group, namely flavin adenine dinucleotide (FAD), which serves as a cofactor in the enzymatic two-electron redox reactions. Nonetheless, prosthetic groups of such enzymes are, in general, electrically well-shielded, and offer no appreciable redox response. We observe that this is also true for the FAD of the immobilized HMTO-ITO electrode, as FAD is electrochemically invisible. The ferricyanide label can be used to quantify the amount of immobilized HMTO on the ITO surface. The formation of coordination bonds between HMTO and ferricyanide was confirmed by comparing the CV diagram of HMTO-ITO with those of other histidine tag-containing proteins. A cell surface receptor (HER2) and formylglycine-generating enzyme (FGE) were employed for the comparison study, as each of these proteins contains a six-histidine tag. As shown in Fig. S5 (Supporting Information), the CV diagrams of HMTO-ITO, HER2-ITO, and FGE-ITO showed only capacitive current flows for the as-prepared electrodes in 0.15 M PBS. After these three electrodes were labeled with ferricyanide, a mixed faradaic current may flow owing to the redox reaction of the adsorbed ferricyanide and also owing to the diffusion of the electroactive ferricyanide in the 0.15 M PBS solution containing 1 mM $Fe(CN)_6^{4-}$/$Fe(CN)_6^{3-}$. All the ferricyanide-labeled electrodes showed typical redox peaks of the adsorbed electroactive species in 0.15 M PBS. Consequently, the redox peaks shown for HMTO-ITO can be attributed to the adsorption of ferricyanide in the surface of HMTO-ITO. For the ferricyanide-labeled HMTO-ITO in PBS solution, Fig. 6b presents the typical CV diagrams of an electroactive-species-adsorbed electrode that features practically zero peak-potential separation and scan-rate-independent characteristics of the peak potentials. In general, the redox peaks caused by adsorbed electroactive species are linearly proportional to the scan rate. The amount of adsorbed HMTO —calculated through the integration of the cathodic peak of the CV diagram, whose electric charge corresponds to 3.3 ± 0.46 μC—was equivalent to 11.4 pmole of HMTO according to Faraday's law, assuming that one ferricyanide may form coordination bonds with two histidine residues of the HMTO histidine tag. As the molecular weight of HMTO is 42 kDa [45], and the Stokes' radius of BSA (66.5 kDa) is known to be 3.48 nm [46], it is estimated that each ferricyanide-labeled HMTO-ITO electrode contains 0.49 μg of electroactive species, and that each HMTO molecule occupies a projected area of approximately 1.52×10^{-13} cm^2. Geometrically, this would indicate that 12.4 pmole of HMTO molecules may be immobilized on an ITO electrode surface having an area of 1.13 cm^2. This result is consistent with our CV measurement of the amount of immobilized HMTO on the ITO electrode.

3.4. Cyclovoltammetric charging/discharging characteristics of biopseudocapacitors

The specific capacity (C g^{-1}) can be calculated using Eq. (1) based on the CV diagram.

$$\mathrm{C} = \frac{Q}{\Delta V \bullet v \bullet m}$$

1

where Q (A s) is half the area of the closed cyclovoltammetric curve. ΔV (V) is the applied potential window. *v* (V s^{-1}) is the scan rate and m (g) is the amount of immobilized enzyme. The ferricyanide-labeled HMTO biopseudocapacitor stores electrical energy mostly in the form of pseudocapacity as shown in Fig. 7a. EDLC only contributes 21.7% of the total capacity of the biopseudocapacitor, as verified by comparing the CV diagram of the nonlabeled HMTO-ITO with that of the ferricyanide-labeled HMTO-ITO. The specific capacity of nonlabeled and labeled HMTO-ITO is measured to be 1.31 C g^{-1} and 6.06 C g^{-1} (or 1.68 mAh g^{-1}), respectively.

The energy and power densities are calculated using Eqs. (2) and (3), respectively [7, 47].

$$\mathrm{E} = \frac{C \bullet \Delta V^2}{2}$$

2

$$\mathrm{P} = \frac{E}{\Delta t}$$

3

where Δt (s) is the discharging time. In general, the specific capacity depends on the potential scan rate, particularly for many metal-oxide-based EDLC electrodes [47]. However, the specific capacity and specific energy of the biopseudocapacitor presented in this work are almost independent of the scan rate (Fig. 7b, see Table S1 for more information about the calculations performed), and the specific power is linearly proportional to the scan rate.

4. Conclusion

An enzyme, a versatile biocatalyst commonly composed of a combination of 20 main amino acids, can be activated with an electrochemical active species to form an activated biomacromolecule and can be used as an electroactive additive providing pseudocapacity in a supercapacitor. In this study, HMTO, an electrically shielded flavoenzyme, is cyclovoltammetrically labeled with ferricyanide and further employed as an electroactive component for a supercapacitor electrode. Strong covalent immobilization of the

enzyme on a transparent electrode via silanization and subsequent amino-glutaraldehyde cross-linking chemistry allows stable and reliable energy storage characteristics of the biopseudocapacitor with minimized influence of the charging/discharging rate on the specific parameters except the specific power. The charge storage capacity of the biopseudocapacitor is currently incomparable to those of conventional EDLC supercapacitors. Nevertheless, we believe that biopseudocapacitors would be potentially available as subsidiary energy storage devices in the near future for various research and industry fields including environment science, human healthcare, and military applications because unique amino acid sequences artificially designed with protein technology could provide various functionalized proteins having properties such as heat or chemical resistivity, light resistivity, substrate selectivity, and mechanical strength in addition to enhanced pseudocapacity. This indicates that electroactive or functionalized proteins immobilized on electrodes can be used in not only traditional biosensor applications but also energy storage devices operated under harsh conditions.

4. Experimental section

2.1. Reagents

HMTO obtained from Hanyang University was stored in a freezer before use (Detailed information about the biosynthesis and purification of HMTO is available elsewhere [48]). ITO electrodes (sheet resistance = 15 Ω sq^{-1}; obtained from Wooyang GMS, Korea) were cut to the dimensions of 20 mm × 17 mm, and initially cleaned with acetone (> 99% obtained from Daejung Chemicals & Metals Co., Ltd.), boiled in ethanol (> 99% obtained from Daejung Chemicals & Metals Co., Ltd.) at 120°C, and washed with distilled water (18.2 MΩ·cm, Direct-Q ultrapure water system, EMD Millipore Corp.). Phosphate-buffered saline (PBS) solution (0.15 M, pH 7), $K_3Fe(CN)_6$, $K_4Fe(CN)_6$, Tris-HCl, and NaCl were purchased from Sigma-Aldrich Co. (St. Louis, MO). 10× Tris-buffered saline was prepared as 50 mM Tris and 15 mM NaCl at pH 6. All the electrochemical reagents were used without further purification.

2.2. Preparation of ferricyanide-labeled HMTO-mediated biopseudocapacitors

Hydrophobic ITO requires multiple pretreatment steps in order to modify the surface for the immobilization of intrinsically hydrophilic enzyme molecules as described in Fig. 1a. We have implemented a common approach to hydroxylate the ITO surface by dipping the substrate in a solution composed of hydrogen peroxide (34.5%, Samchun Pure Chemicals Co., Ltd.), ammonium hydroxide (28–30%, Sigma-Aldrich Co.), and distilled water (volume ratio = 1:1:5) for 30 min at 60°C [49, 50]. The hydroxylated ITO (HO-ITO) surface provides a better environment for the following silanization process, which is accomplished by immersing the HO-ITO in a 2.0% solution of APTES (≥ 98%, Sigma-Aldrich Co.) in anhydrous toluene (99.8%, Sigma-Aldrich Co.) for 48 h at 70°C. After thorough rinsing with anhydrous toluene, the silanized ITO (APTES-ITO) is fully dried using N_2 gas blowing. Glutaraldehyde (GA) (70% in H_2O, Sigma-Aldrich Co.) reacts directly with the primary amine end of APTES to form an imine compound. This is performed simply by immersing the APTES-ITO into a 2.5% GA solution in 0.1 M PBS (pH 7.0) for

2 h at room temperature. Finally, 100 µL of N-methyl tryptophan oxidase solution (10 µL enzyme solution + 90 µL 1× Tris-buffered saline solution (pH 6)) is carefully pipetted onto the GA-ITO surface and stored overnight at 4°C. Unspecified aldehyde ends are blocked with a 0.15 M PBS solution (pH 7) containing 1 mg mL^{-1} bovine serum albumin (BSA) (≥ 98%, Sigma-Aldrich Co.) for 1 h at room temperature. Note that the actual size of HMTO (42 kDa) is smaller than that of BSA (66.5 kDa) considering that the Stokes' radius of BSA is 3.48 nm [46]. Finally, the immobilized HMTO is electrochemically activated via CV in a 0.15 M PBS (pH 7) solution containing 1 mM $Fe(CN)_6^{4-}/Fe(CN)_6^{3-}$ at a scan rate of 10 mV s^{-1} and thoroughly rinsed with distilled water. The working mechanism of the ferricyanide-labeled HMTO-mediated biopseudocapacitor is shown in Fig. 1b. The nonfaradaic EDLC portion caused by the aligned charge accumulation and the faradaic pseudocapacity portion caused by the redox reaction of the ferricyanide-labeled HMTO collectively contribute to the total capacity of the biopseudocapacitor. Electrons exchanged in the redox reaction of ferricyanide/ferrocyanide redox couple can move from (in an electroreduction) or to (in an electrooxidation) the electrode substrate through the thin APTES-GA layer via tunneling.

2.3. Equipment and electrochemical measurements

CV and EIS measurements were obtained in a three-electrode aqueous system using a potentiostat/galvanostat (Reference 600™, Gamry Instruments) and a laboratory-made Teflon® electrochemical cell (Fig. S1, Supporting Information). A Pt wire (99.95%) and sodium-chloride-saturated Ag/AgCl electrode were used as the counter and reference electrodes, respectively. A 0.15 M PBS solution (pH 7) was used as a supporting electrolyte with or without 1 mM $Fe(CN)_6^{3-}/Fe(CN)_6^{4-}$ in total electroactive species. The CV diagrams were obtained at the scan rates of 10, 20, 50, 80, 100, 150, and 250 mV s^{-1}. The frequency range and amplitude of the EIS spectra were 100 mHz–100 kHz and 5 mV, respectively. The bias potential (V_{DC}) of EIS in the presence of $Fe(CN)_6^{3-}/Fe(CN)_6^{4-}$ for bare ITO, HO-ITO, and APTES-ITO was 0.22 V vs. Ag/AgCl, whereas the corresponding values for GA-ITO and HMTO-ITO were 0.29 V vs. Ag/AgCl and 0.275 V vs. Ag/AgCl, respectively. V_{DC} in the absence of $Fe(CN)_6^{3-}/Fe(CN)_6^{4-}$ was the open-circuit potential, i.e., -0.6 V vs. Ag/AgCl. Furthermore, surface analyses data were obtained from AFM (NTEGRA Prima TS-150, NT-MDT), ATR-FTIR (Nicolet 6700, Thermo Scientific, Ge window), and Raman spectroscopy (LabRam Aramis IR2, Horiba).

Declarations

Acknowledgments

This work was supported by the National Research Foundation (NRF) (grant number 2021R1/1A2059854) of Korea.

References

1. J. Eskusson, P. Rauwel, J. Nerut, A. Janes, A Hybrid Capacitor Based on Fe3O4-Graphene Nanocomposite/Few-Layer Graphene in Different Aqueous Electrolytes, J Electrochem Soc, 163 (2016) A2768-A2775.
2. H.H. Zhang, M.M. Yao, J.B. Wei, Y.W. Zhang, S.T. Zhang, Y. Gao, J.Y. Li, P. Lu, B. Yang, Y.G. Ma, Stable p/n-Dopable Conducting Redox Polymers for High-Voltage Pseudocapacitor Electrode Materials: Structure-Performance Relationship and Detailed Investigation into Charge-Trapping Effect, Adv Energy Mater, 7 (2017).
3. A. Kumar, R.K. Sharma, G. Singh, S. Umapathy, P.R. Kharangarh, High Performance Pseudocapacitor Electrode Materials Based on CoCl2 Doped Graphene Quantum Dots, Emerg Mater Res, 6 (2017).
4. K.-S. Põder, J. Eskusson, E. Lust, A. Jänes, Non-Aqueous Zn-Ion Hybrid Supercapacitors: Acetonitrile vs Propylene Carbonate Based Electrolyte, J Electrochem Soc, 170 (2023) 060501.
5. Y. Dai, W. Li, Z. Chen, X. Zhu, J. Liu, R. Zhao, D.S. Wright, A. Noori, M.F. Mousavi, C. Zhang, An air-stable electrochromic conjugated microporous polymer as an emerging electrode material for hybrid energy storage systems, J. Mater. Chem. A, 7 (2019) 16397–16405.
6. J. Ahn, Y. Song, Y.J. Kim, D. Nam, T. Kim, K. Kwak, C.H. Kwon, Y. Ko, S.J. Lee, J. Cho, Redox-active ligand-mediated assembly for high-performance transition metal oxide nanoparticle-based pseudocapacitors, Chemical Engineering Journal, 455 (2023) 140742.
7. B.E. Conway, Electrochemical supercapacitors: scientific fundamentals and technological applications, Plenum Press, New York, 1999.
8. D.W. Lee, J.H. Lee, N.K. Min, J.H. Jin, Buckling Structured Stretchable Pseudocapacitor Yarn, Sci Rep-Uk, 7 (2017).
9. E. Gonzalez-Arribas, O. Aleksejeva, T. Bobrowski, M.D. Toscano, L. Gorton, W. Schuhmann, S. Shleev, Solar biosupercapacitor, Electrochem Commun, 74 (2017) 9–13.
10. D. Pankratov, F. Conzuelo, P. Pinyou, S. Alsaoub, W. Schuhmann, S. Shleev, A Nernstian Biosupercapacitor, Angew Chem Int Edit, 55 (2016) 15434–15438.
11. S. Shleev, E. Gonzalez-Arribas, M. Falk, Biosupercapacitors, Curr Opin Electroche, 5 (2017) 226–233.
12. E. Gonzalez-Arribas, M. Falk, O. Aleksejeva, S. Bushnev, P. Sebastian, J.M. Feliu, S. Shleev, c:/ A conventional symmetric biosupercapacitor based on rusticyanin modified gold electrodes, J Electroanal Chem, 816 (2018) 253–258.
13. X.X. Xiao, E. Magner, A quasi-solid-state and self-powered biosupercapacitor based on flexible nanoporous gold electrodes, Chem Commun, 54 (2018) 5823–5826.
14. T. Bobrowski, E.G. Arribas, R. Ludwig, M.D. Toscano, S. Shleev, W. Schuhmann, Rechargeable, flexible and mediator-free biosupercapacitor based on transparent ITO nanoparticle modified electrodes acting in mu M glucose containing buffers, Biosens Bioelectron, 101 (2018) 84–89.
15. M. Ramesh, P. Balakrishnan, S. Dhanaprabhu, A. Ravanan, J. Maniraj, Enzyme-modified electrodes for biofuel cells: A comprehensive review, Materials Today: Proceedings, 46 (2021) 3495–3501.

16. L. Sun, W. Li, M. Wang, W. Ding, Y. Ji, Development of an electrochemical impedance immunosensor for myoglobin determination, International Journal of Electrochemical Science, 12 (2017) 6170–6179.
17. P. Khanna, M.S. Jorns, N-methyltryptophan oxidase from Escherichia coli: Reaction kinetics with N-methyl amino acid and carbinolamine substrates, Biochemistry-Us, 40 (2001) 1451–1459.
18. E.C. Ralph, P.F. Fitzpatrick, pH and kinetic isotope effects on sarcosine oxidation by N-methyltryptophan oxidase, Biochemistry-Us, 44 (2005) 3074–3081.
19. S.L. Rice, M.R. Preimesberger, E.A. Johnson, J.T.J. Lecomte, Introduction of a covalent histidine-heme linkage in a hemoglobin: A promising tool for heme protein engineering, J Inorg Biochem, 141 (2014) 198–207.
20. W.B. Lutz, K. Folkers, Advantages of Ferric Ferricyanide to Detect Certain Peptides and Proteins on Chromatograms, Anal Biochem, 120 (1982) 410–413.
21. G.B. Postnikova, S.A. Moiseeva, E.A. Shekhovtsova, E.V. Goraev, V.S. Sivozhelezov, Ferrocyanide - a novel catalyst for oxymyoglobin oxidation by molecular oxygen, Febs J, 274 (2007) 5360–5369.
22. R. Blankespoor, B. Limoges, B. Schollhorn, J.L. Syssa-Magale, D. Yazidi, Dense monolayers of metal-chelating ligands covalently attached to carbon electrodes electrochemically and their useful application in affinity binding of histidine-tagged proteins, Langmuir, 21 (2005) 3362–3375.
23. A.M. Shanmugharaj, J.H. Bae, K.Y. Lee, W.H. Noh, S.H. Lee, S.H. Ryu, Physical and chemical characteristics of multiwalled carbon nanotubes functionalized with aminosilane and its influence on the properties of natural rubber composites, Compos Sci Technol, 67 (2007) 1813–1822.
24. A. Tiwari, S.R. Dhakate, Chitosan-SiO2-multiwall carbon nanotubes nanocomposite: A novel matrix for the immobilization of creatine amidinohydrolase, Int J Biol Macromol, 44 (2009) 408–412.
25. M.Z. Iqbal, M.S. Katsiotis, S.M. Alhassan, M.W. Liberatore, A.A. Abdala, Effect of solvent on the uncatalyzed synthesis of aminosilane-functionalized graphene, Rsc Adv, 4 (2014) 6830–6839.
26. N. Chauhan, J. Narang, Sunny, C.S. Pundir, Immobilization of lysine oxidase on a gold-platinum nanoparticles modified Au electrode for detection of lysine, Enzyme Microb Tech, 52 (2013) 265–271.
27. C. Weigel, R. Kellner, Ftir-Atr-Spectroscopic Investigation of the Silanization of Germanium Surfaces with 3-Aminopropyltriethoxysilane, Fresen Z Anal Chem, 335 (1989) 663–668.
28. L.R. Knopke, N. Nemati, A. Kockritz, A. Bruckner, U. Bentrup, Reaction Monitoring of Heterogeneously Catalyzed Hydrogenation of Imines by Coupled ATR-FTIR, UV/Vis, and Raman Spectroscopy, Chemcatchem, 2 (2010) 273–280.
29. S.K. Arya, A.K. Prusty, S.P. Singh, P.R. Solanki, M.K. Pandey, M. Datta, B.D. Malhotra, Cholesterol biosensor based on N-(2-aminoethyl)-3-aminopropyl-trimethoxysilane self-assembled monolayer, Anal Biochem, 363 (2007) 210–218.
30. C. Dhand, P.R. Solanki, K.N. Sood, M. Datta, B.D. Malhotra, Polyaniline nanotubes for impedimetric triglyceride detection, Electrochem Commun, 11 (2009) 1482–1486.

31. M.C. Chang, J. Tanaka, FT-IR study for hydroxyapatite/collagen nanocomposite cross-linked by glutaraldehyde, Biomaterials, 23 (2002) 4811–4818.
32. H. Gaspar, C. Pereira, S.L.H. Rebelo, M.F.R. Pereira, J.L. Figueiredo, C. Freire, Understanding the silylation reaction of multi-walled carbon nanotubes, Carbon, 49 (2011) 3441–3453.
33. S.M. Park, J.S. Yoo, Electrochemical impedance spectroscopy for better electrochemical measurements, Anal Chem, 75 (2003) 455a-461a.
34. W.J. Gao, S. Cao, Y.Z. Yang, H. Wang, J. Li, Y.M. Jiang, Electrochemical impedance spectroscopy investigation on indium tin oxide films under cathodic polarization in NaOH solution, Thin Solid Films, 520 (2012) 6916–6921.
35. J. Bisquert, Theory of the impedance of electron diffusion and recombination in a thin layer, J Phys Chem B, 106 (2002) 325–333.
36. Q. Wang, S. Ito, M. Gratzel, F. Fabregat-Santiago, I. Mora-Sero, J. Bisquert, T. Bessho, H. Imai, Characteristics of high efficiency dye-sensitized solar cells, J Phys Chem B, 110 (2006) 25210–25221.
37. F. Fabregat-Santiago, J. Bisquert, G. Garcia-Belmonte, G. Boschloo, A. Hagfeldt, Influence of electrolyte in transport and recombination in dye-sensitized solar cells studied by impedance spectroscopy, Sol Energ Mat Sol C, 87 (2005) 117–131.
38. M.E. Winkler, R.D. Bereman, Stereoelectronic Properties of Metalloenzymes.6. Effects of Anions and Ferricyanide on the Copper(Ii) Site of the Histidine and the Tryptophan Modified Forms of Galactose-Oxidase, J Am Chem Soc, 102 (1980) 6244–6247.
39. J.L. Sun, S.J. Hao, M. Radle, W. Xu, I. Shelaev, V. Nadtochenko, V. Shuvalov, A. Semenov, H. Gordon, A. van der Est, J.H. Golbeck, Evidence that histidine forms a coordination bond to the A(0A) and A(0B) chlorophylls and a second H-bond to the A(1A) and A(1B) phylloquinones in M688H(PsaA) and M668H(PsaB) variants of Synechocystis sp PCC 6803, Bba-Bioenergetics, 1837 (2014) 1362–1375.
40. P. Cordoba-Torres, M. Keddam, R.P. Nogueira, On the intrinsic electrochemical nature of the inductance in EIS A Monte Carlo simulation of the two-consecutive-step mechanism: The flat surface 2 D case, Electrochim Acta, 54 (2008) 518–523.
41. P. Cordoba-Torres, M. Keddam, R.P. Nogueira, On the intrinsic electrochemical nature of the inductance in EIS-A Monte Carlo simulation of the two-consecutive steps mechanism: The rough 3D case and the surface relaxation effect, Electrochim Acta, 54 (2009) 6779–6787.
42. F. Seland, R. Tunold, D.A. Harrington, Impedance study of methanol oxidation on platinum electrodes, Electrochim Acta, 51 (2006) 3827–3840.
43. B.P.G. Silva, D.Z. de Florio, S. Brochsztain, Characterization of a Perylenediimide Self-Assembled Monolayer on Indium Tin Oxide Electrodes Using Electrochemical Impedance Spectroscopy, J Phys Chem C, 118 (2014) 4103–4112.
44. S.J. Konopka, B. Mcduffie, Diffusion Coefficients of Ferricyanide and Ferrocyanide Ions in Aqueous Media, Using Twin-Electrode Thin-Layer Electrochemistry, Anal Chem, 42 (1970) 1741-&.

45. A. Ilari, A. Bonamore, S. Franceschini, A. Fiorillo, A. Boffi, G. Colotti, The X-ray structure of N-methyltryptophan oxidase reveals the structural determinants of substrate specificity, Proteins, 71 (2008) 2065–2075.
46. I. Axelsson, Characterization of Proteins and Other Macromolecules by Agarose-Gel Chromatography, J Chromatogr, 152 (1978) 21–32.
47. J. Gomez, E.E. Kalu, High-performance binder-free Co-Mn composite oxide supercapacitor electrode, J Power Sources, 230 (2013) 218–224.
48. H. Cho, J. Jaworski, A portable and chromogenic enzyme-based sensor for detection of abrin poisoning, Biosens Bioelectron, 54 (2014) 667–673.
49. C.O. Kim, S.Y. Hong, M. Kirn, S.M. Park, J.W. Park, Modification of indium-tin oxide (ITO) glass with aziridine provides a surface of high amine density, J Colloid Interf Sci, 277 (2004) 499–504.
50. E. Zor, I.H. Patir, H. Bingol, M. Ersoz, An electrochemical biosensor based on human serum albumin/graphene oxide/3-aminopropyltriethoxysilane modified ITO electrode for the enantioselective discrimination of D- and L-tryptophan, Biosens Bioelectron, 42 (2013) 321–325.

Figures

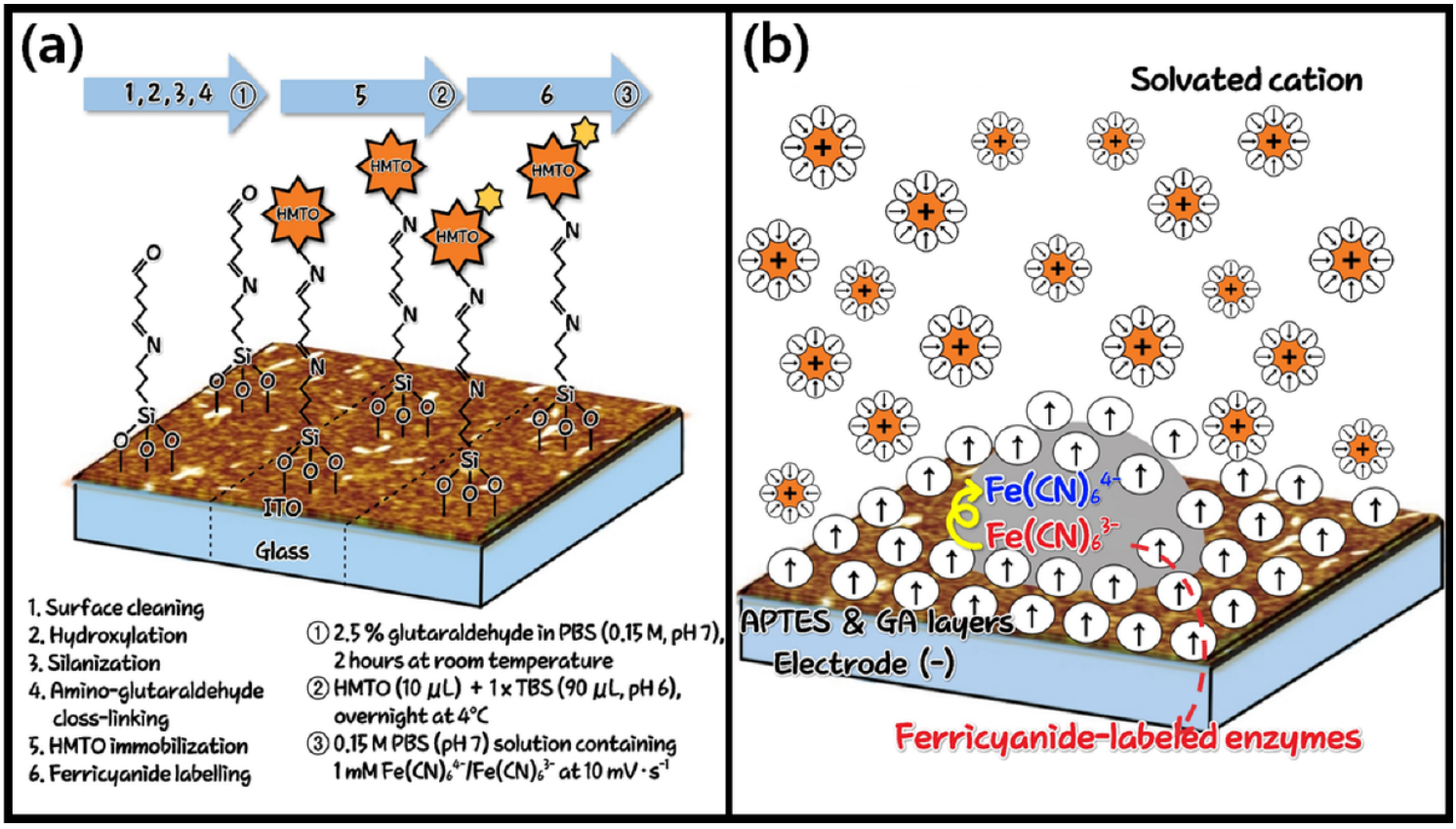

Figure 1

Schematic drawing of (a) the step-by-step preparation of the FC (ferricyanide)-labeled biopseudocapacitor including the cleaning of the ITO surface, hydroxylation, silanization, amino-

glutaraldehyde cross-linking, HMTO immobilization, blocking excess glutaraldehyde with BSA, and fixation of FC redox species, and (b) illustrative cross-section of the biopseudocapacitor when a cathodic potential is applied. Note that both the EDLC capacity (between the electrode and electrolyte) and pseudocapacity (between the electrode and the FC-labelled HMTO) occur simultaneously.

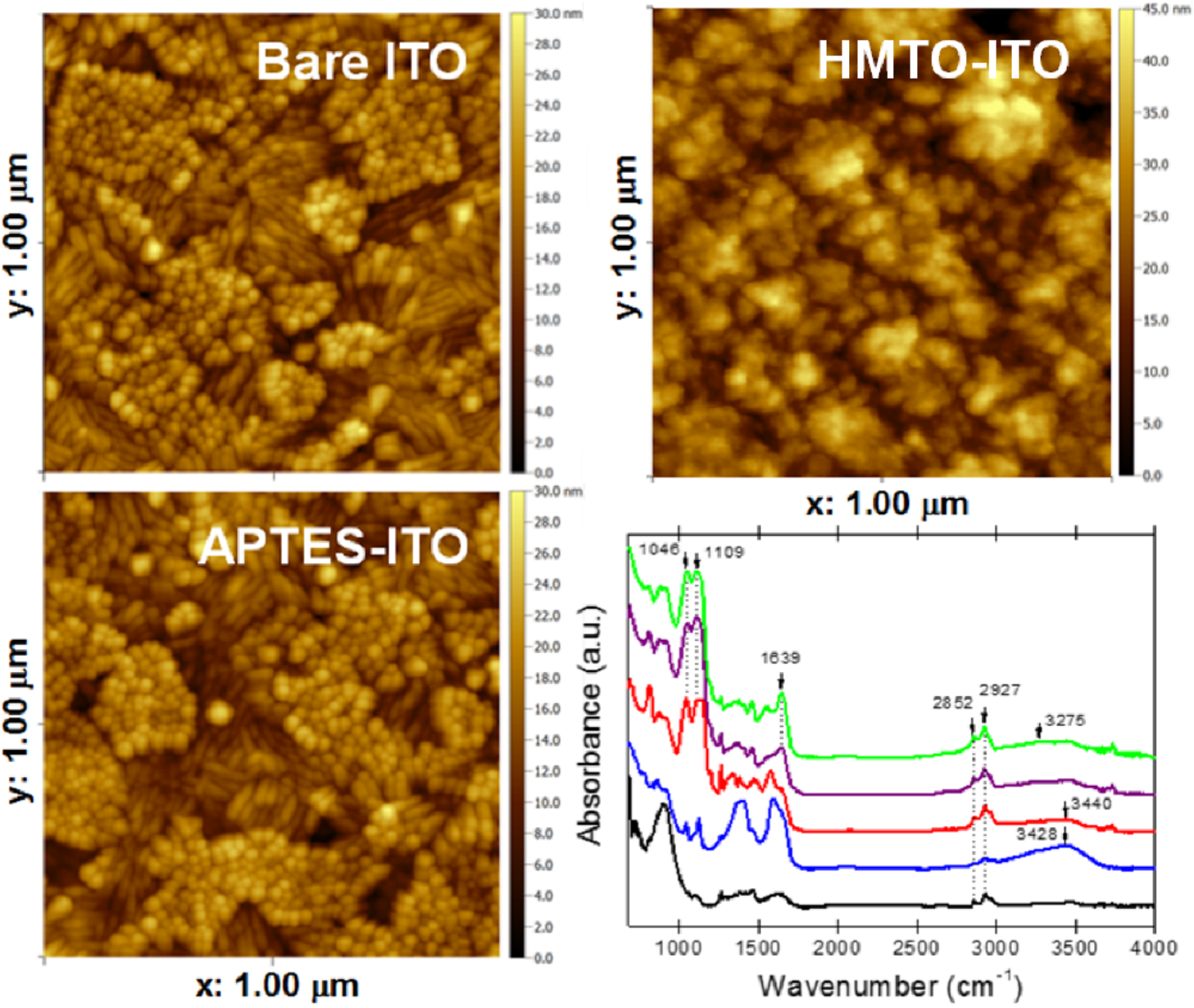

Figure 2

AFM images of bare ITO, APTES-ITO, and HMTO-ITO with spectrum-density-based total root-mean-square roughness of 7.469, 6.774, and 8.295 nm, respectively. The corresponding ATR-FTIR spectra (reflection mode) are presented: black, blue, red, purple, and green lines represent bare ITO as background, HO-ITO, APTES-ITO, GA-ITO, and HMTO-ITO, respectively. Note that the peak shown at 1639 cm^{-1} assigned to an imine vibration was more enhanced for the GA-ITO and HMTO-ITO electrodes compared with the others.

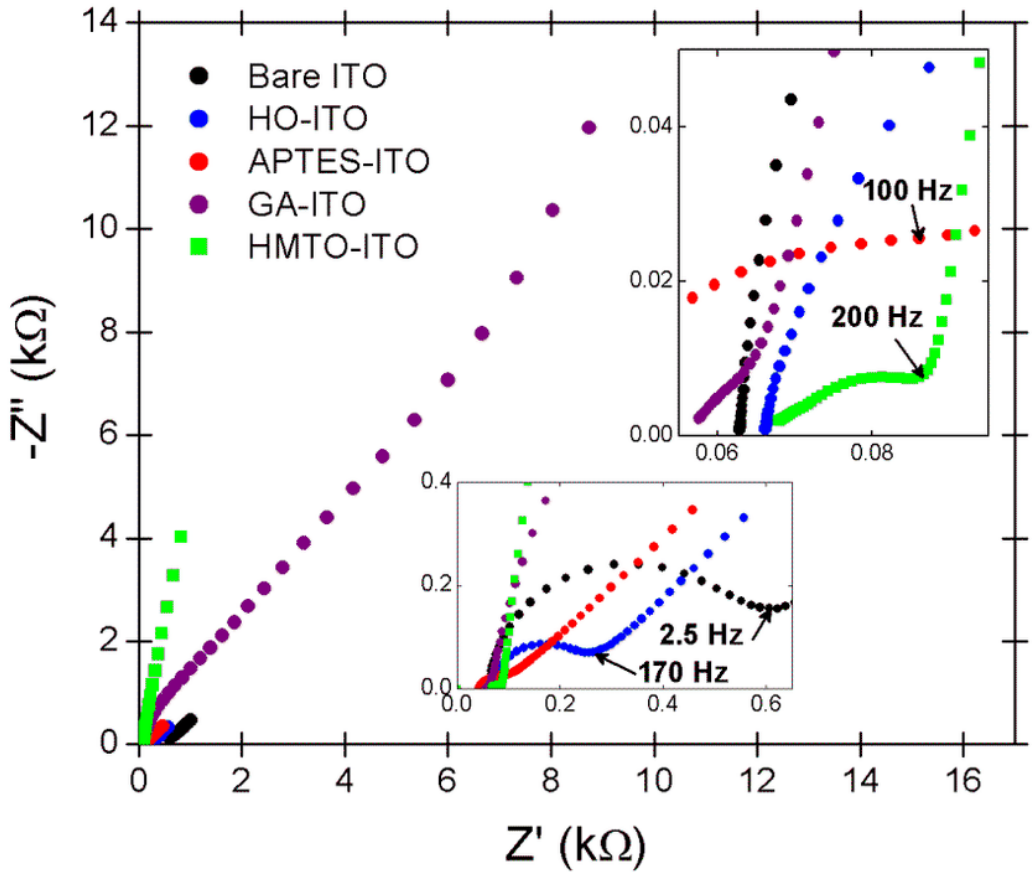

Figure 3

EIS spectra of bare ITO, HO-ITO, APTES-ITO, GA-ITO, and HMTO-ITO substrates in a 0.15 M PBS solution (pH 7) containing a 1 mM $Fe(CN)_6^{3-}/Fe(CN)_6^{4-}$ redox couple: frequency range = 100 mHz–100 kHz; amplitude = 5 mV; V_{DC} for bare ITO, HO-ITO, and APTES-ITO = 0.22 V vs. Ag/AgCl; V_{DC} for GA-ITO = 0.29 V vs. Ag/AgCl; V_{DC} for HMTO-ITO = 0.275 V vs. Ag/AgCl. Note that the R_s of each substrate varies with the electrochemical cell-to-cell variations. Furthermore, the semicircle diameter in the high-frequency region decreases from 579 W for bare ITO to 33 W for APTES-ITO.

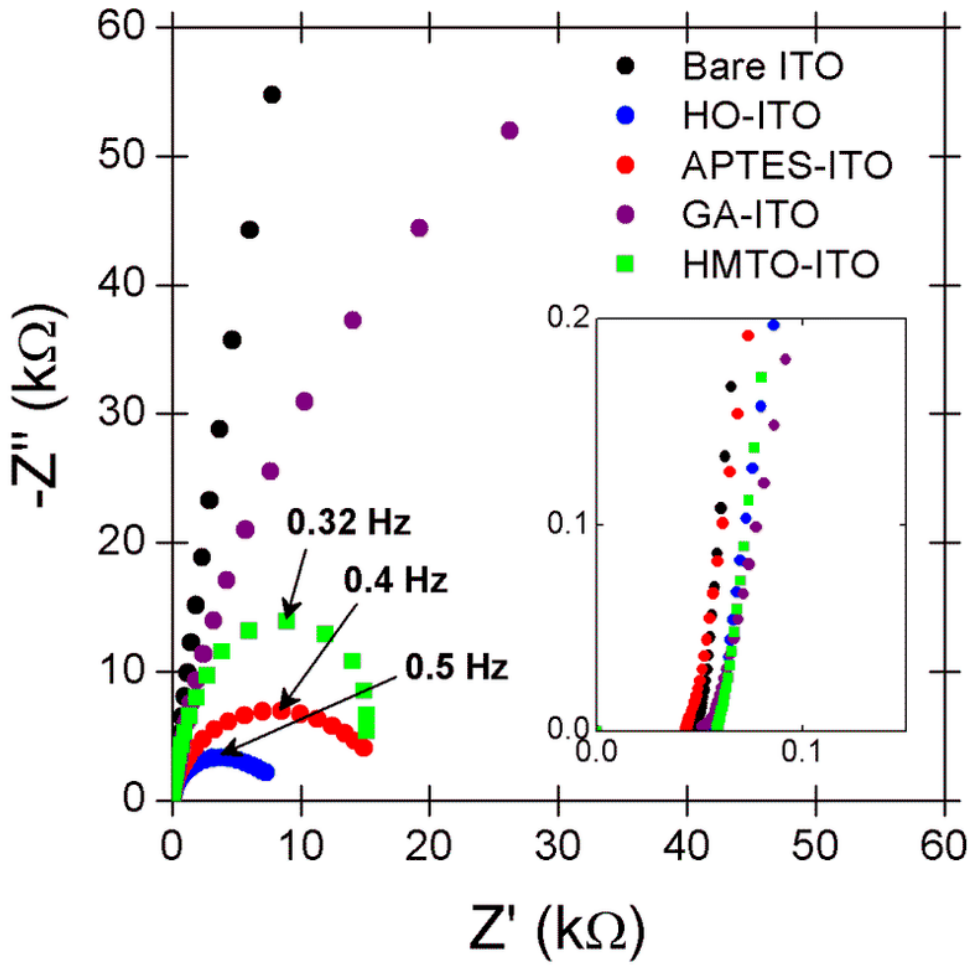

Figure 4

EIS spectra of bare ITO, HO-ITO, APTES-ITO, GA-ITO, and HMTO-ITO substrates in a 0.15 M PBS solution (pH 7): frequency range = 100 mHz–100 kHz; amplitude = 5 mV; V_{DC} = -0.6 V vs. Ag/AgCl. Note that the R_s of each substrate varies with the electrochemical cell-to-cell variations.

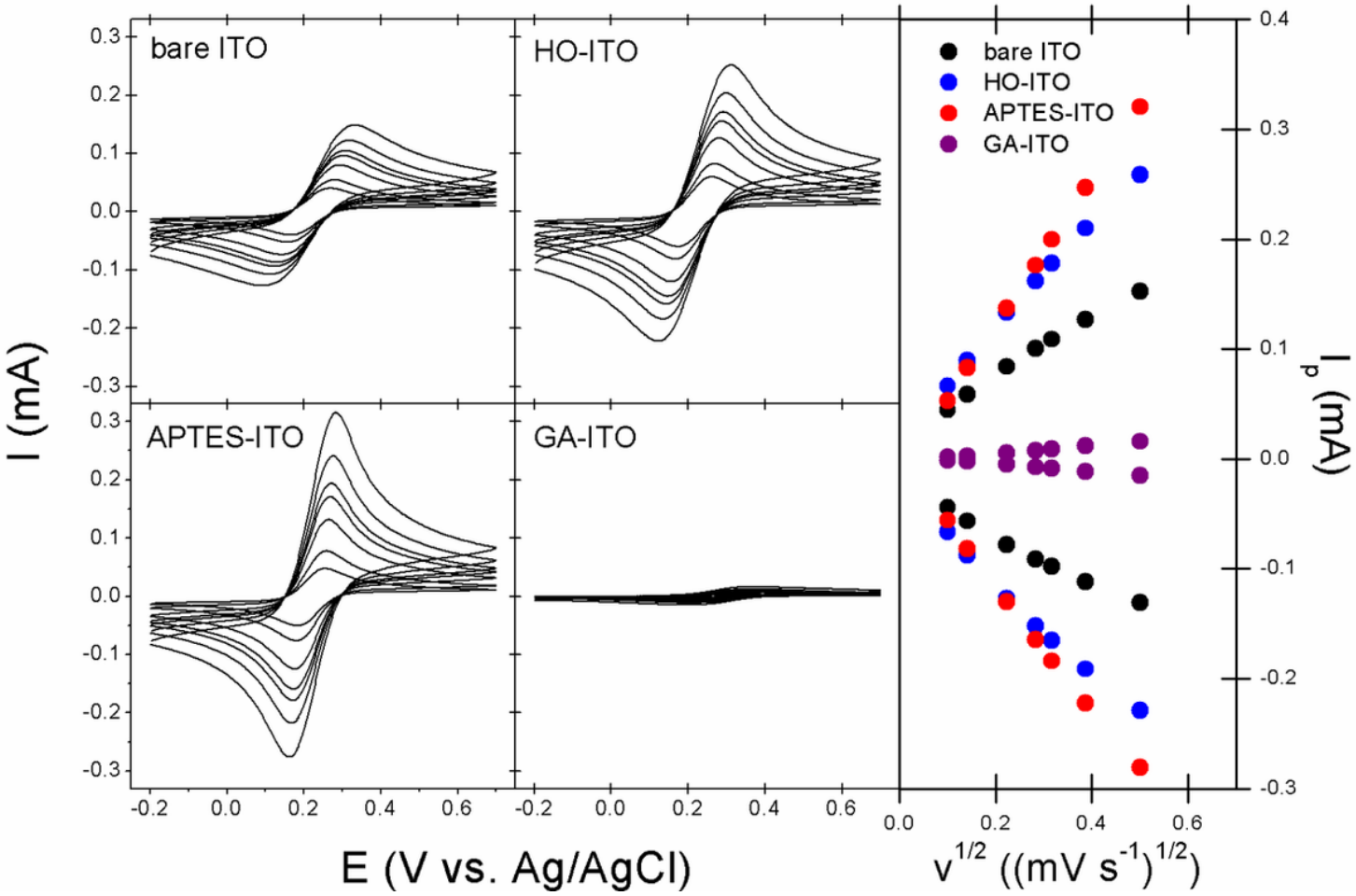

Figure 5

CV diagrams of bare ITO, HO-ITO, APTES-ITO, and GA-ITO substrates in a 0.15 M PBS (pH 7) solution containing 1 mM $Fe(CN)_6^{4-}$/$Fe(CN)_6^{3-}$ at the scan rates of 10, 20, 50, 80, 100, 150, and 250 mV s^{-1}. The plot of the peak current as a function of the square root of the scan rate is a straight line directly related to the electrochemical active area of the electrode.

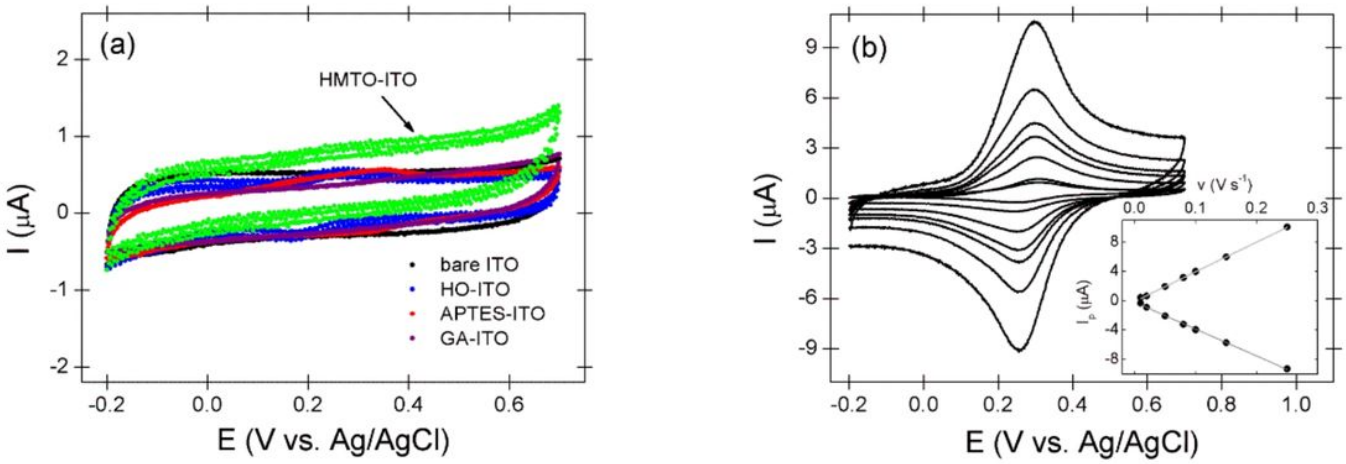

Figure 6

(a) CV diagrams of bare ITO, HO-ITO, APTES-ITO, GA-ITO, and HMTO-ITO substrates in a 0.15 M PBS (pH 7) solution at a scan rate of 50 mV s^{-1}. (b) CV diagrams of the ferricyanide-labeled HMTO-ITO substrate in a 0.15 M PBS (pH 7) solution at the scan rates of 10, 20, 50, 80, 100, 150, and 250 mV s^{-1}. The plot of the peak current as a function of the scan rate is a straight line, indicating that the redox peaks are caused by the adsorbed electroactive species. Note that the abscissa can be converted into a time axis by dividing it by the applied scan rate, and the amount of adsorbate on the ITO substrate can be calculated from the peak area of each voltammogram, which was 3.3 ± 0.46 mC.

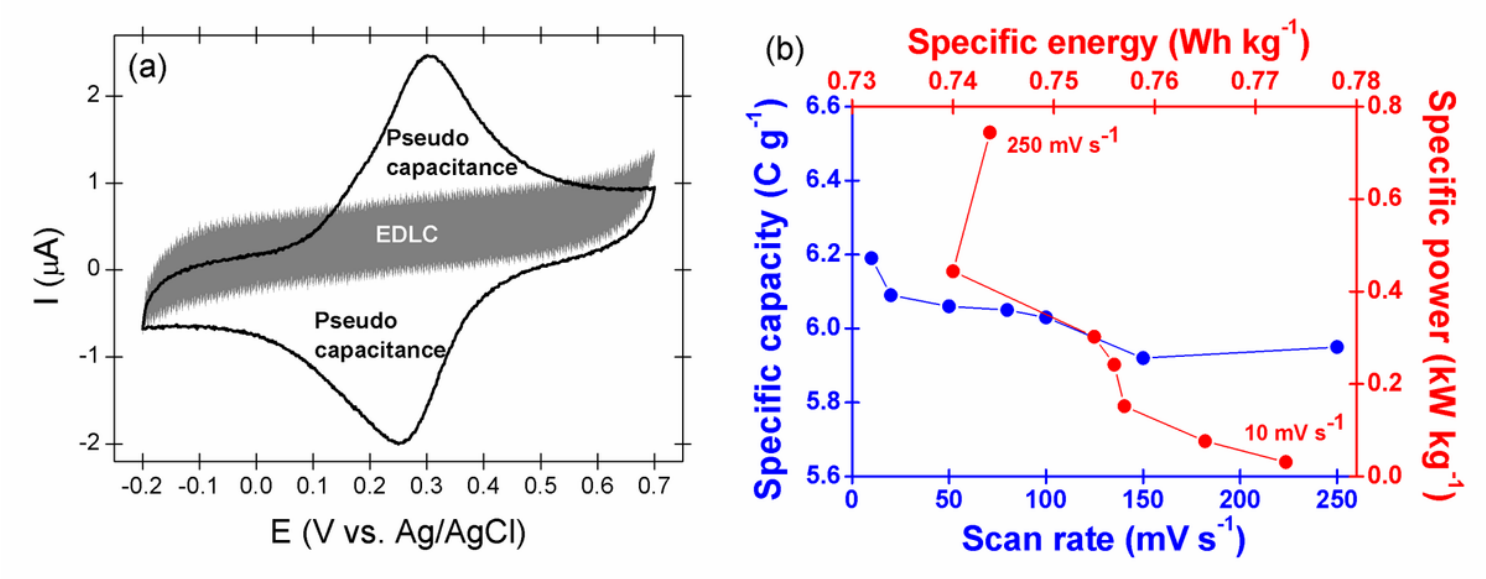

Figure 7

CV diagrams of nonlabeled (shaded) and ferricyanide-labeled (solid line) HMTO-ITO electrodes in a 0.15 M PBS (pH 7) solution at a scan rate of 50 mV s^{-1} (a) and variations of the specific capacity, energy, and power densities as the scan rate increases from 10 to 250 mV s^{-1} (b). Note that the specific parameters at each scan rate are determined from the CV diagrams shown in Fig. 6b.

Supplementary Files

This is a list of supplementary files associated with this preprint. Click to download.

- Supplementarymaterial.docx